TITLE PAGE

Report Title: **Novel Approaches to High-Efficiency III-V Nitride Heterostructure Emitters for Next-Generation Lighting Applications**

Type of Report: Annual

Reporting Period Start Date: October 2004

Reporting Period End Date: September 2005

Principal Author(s): Russell D. Dupuis

Date Report was Issued: January 2006

DOE Award Number: DE-FC26-03NT41946

Name and Address of Submitting Organization: Georgia Institute of Technology
Atlanta, Georgia 30332

Name, phone number and fax number of preparer: Russell D. Dupuis
404 385-6094 and 404 385-6096 (Fax)

"This report was prepared as an account of work sponsored by an agency of the United States Government. Neither the United States Government nor any agency thereof, nor any of their employees, makes any warranty, express or implied, or assumes any legal liability or responsibility for the accuracy, completeness, or usefulness of any information, apparatus, product, or process disclosed, or represents that its use would not infringe privately owned rights. Reference herein to any specific commercial product, process, or service by trade name, trademark, manufacturer, or otherwise does not necessarily constitute or imply its endorsement, recommendation, or favoring by the United States Government or any agency thereof. The views and opinions of authors expressed herein do not necessarily state or reflect those of the United States Government or any agency thereof."

ABSTRACT

We report research activities and technical progress on the development of high-efficiency long wavelength (λ~540nm) green light emitting diodes which covers the second year of the three-year program "Novel approaches to high-efficiency III-V nitride heterostructure emitters for next-generation lighting applications". The second year activities were focused on the development of *p*-type layer that has less/no detrimental thermal annealing effect on green LED active region as well as excellent structural and electrical properties and the development of green LED active region that has superior luminescence quality for λ~540nm green LEDs. We have also studied the thermal annealing effect on blue and green LED active region during the *p*-type layer growth. As a progress highlight, we obtained green-LED-active-region-friendly $In_{0.04}Ga_{0.96}N$:Mg exhibiting low resistivity with higher hole concentration ($p=2.0\times10^{18}$ cm^{-3} and a low resistivity of 0.5 Ω-cm) and improved optical quality green LED active region emitting at λ~540nm by electroluminescence. The active region of the green LEDs was found to be much more sensitive to the thermal annealing effect during the *p*-type layer growth than that of the blue LEDs. We have designed grown, fabricated green LED structures for both 520 nm and 540 nm for the evaluation of second year green LED development.

TABLE OF CONTENTS

LIST OF GRAPHICAL MATERIALS ---------- 4

INTRODUCTION ---------- 6

EXECUTIVE SUMMARY ---------- 9

EXPERIMENTAL ---------- 11

RESULTS AND DISCUSSION ---------- 13

CONCLUSION ---------- 22

LIST OF ACRONYMS AND ABBREBIATIONS ---------- 23

BIBLIOGRAPHY ---------- 24

REFERENCES ---------- 25

LIST OF GRAPHICAL MATERIALS

Figure 1: Bandgap energy vs. lattice constant of III-V semiconductor materials for visible light-emitting device applications.

Figure 2: Conversion efficiency vs. wavelength for current generation light-emitting diodes.

Figure 3: Measured hole concentration, mobility, and resistivity of *p-In0.04Ga0.99N:Mg* and *p-GaN:Mg* samples.

Figure 4: Measured hole concentration, mobility, and resistivity of *p-GaN:Mg* at 930oC with different growth rate.

Figure 5: The AFM images with the 5×5 µm2 scans of *p-In0.04Ga0.99N:Mg* and *p-GaN:Mg* samples.

Figure 6: PL intensity change with peak wavelength increase from InGaN/GaN MQWs for (a) the first batch and (b) the second batch of green LED MQW active region optimization.

Figure 7: EL intensity change with increasing injection current from InGaN/GaN MQWs of 520nm green LED MQW by quick EL test.

Figure 8: EL intensity change with increasing injection current from InGaN/GaN MQWs of 540nm green LED MQW by quick EL test.

Figure 9: Summary of the structural, electrical, and optical characterization results for the green LED structures.

Figure 10: Cross-sectional transmission electron microscopy of MQW active layers for LEDs with (a) *p-GaN* and (b) *p-In0.04Ga0.96N* layers.

Figure 11: Electron holography of MQW active layers for LEDs with *p-In0.04Ga0.96N* layers.

Figure 12: Room-temperature PL wavelength and intensity of MQW and LED samples (d), (e), (f), and (g).

Figure 13: Room-temperature PL wavelength shift and relative intensity ratio of blue and green LEDs.

Figure 14: The room-temperature EL spectra of LED Sample (e) and (f) at low current level.

Figure 15: The room-temperature EL spectra of LED Sample (e) and (f) at high current level.

Figure 16: Current-voltage characteristics of green LEDs with different *p-layers* at room temperature.

Figure 17: (a) Schematic epitaxial structure of the green LEDs grown for the optical power measurement and internal quantum efficiency evaluation and (b) Bright luminescence emitting at 540nm from green LED epitaxial structure by EL quick test.

INTRODUCTION

While great success has recently been achieved in the development of III-N visible light-emitting diodes (LEDs) and lasers in the violet and blue spectral region (λ~400-480nm), less success has been demonstrated in obtaining high-internal quantum efficiency LEDs emitting in the UV and the green spectral regions, i.e., for light-emitting diodes operating in the wavelength range of λ=280-390nm and 530-560nm. We proposed to develop improved green LEDs in this program that are required for a variety of applications, in particular, for efficient, low-cost solid-state white and colored lighting.

Most blue and green LEDs made today are manufactured from the InAlGaN system while the yellow, orange and red LEDs are made from the InAlGaP system, as shown in Figure 1. The internal quantum efficiency of the best green LEDs is still well below that of the best blue LEDs and the efficiency is even lower for longer wavelengths in the yellow. For example, as Krames has reported that currently, the internal quantum efficiency (IQE, η_{int}) of blue LED materials emitting at λ~460nm is ~60% while the IQE of a green LED emitting at λ~525nm is only ~25%, and only ~10% at λ~545nm. Also, the IQE of typical yellow InAlGaP materials emitting at ~590nm is only about 10%[1]. This performance deficiency is often referred to as "the green gap", as shown in Figure 2. Since the internal quantum efficiency of current red LED InAlGaP materials is estimated to be ~90%[1], there is still much room for the improvement of the performance of longer-wavelength pure green and yellow LEDs. Although the best LED performance has been improving with time, the η_{int} of the best LEDs with longer visible wavelength are still significantly worse than the best blue devices.

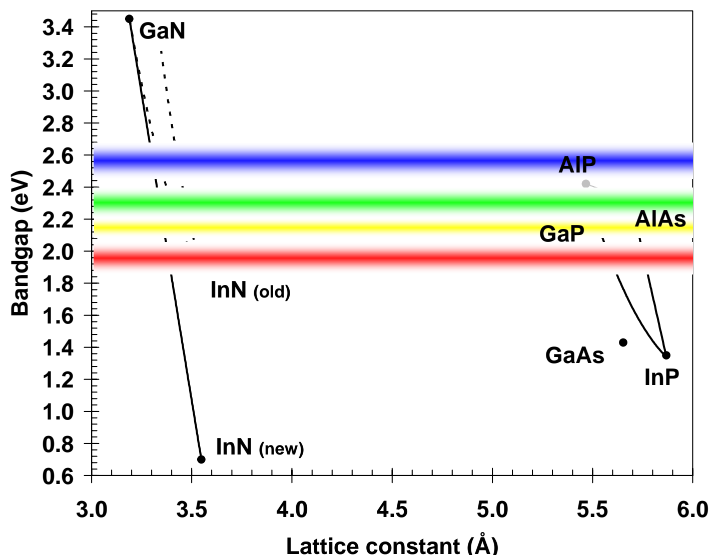

Figure 1: Bandgap energy vs. lattice constant of III-V semiconductor materials for visible light-emitting device applications.

Recently, binary InN single crystals were reported to have a fundamental bandgap energy of 0.65~0.9eV[2] which is dramatically lower than previously reported at 1.89eV (see Figure 1). The recent reports provide new possibilities for InGaN LEDs having green, amber, and red colors with less-than-previously-thought indium composition in the InGaN quantum-well (QW) active layers, indicating less-than-previously-estimated strains.

GaN-based Group III-nitride wide bandgap semiconductor material systems[3] have brought innovative changes in photonic devices, which enable LEDs operating wavelengths to extend into the ultraviolet (UV) spectral region. However, the largest impact to date for III-N LEDs has been from the blue to green visible spectral region which was earlier covered by conventional GaP- and InAlGaP-

based III-V semiconductor material systems. Because no LED device previously covered the blue visible-spectral region, the emergence of III-nitride materials has had an especially tremendous impact on the performance of blue-spectrum LEDs. Adding efficient blue LEDs fills the missing element of the RGB (red-green-blue) primary color elements, which has opened up new opportunities for high-performance solid-state white-light illumination systems[4] and LED-based full-color display systems. Figure 1 shows the bandgap energy of the III-V semiconductor materials that are useful for visible light-emitting device applications. The development of visible LEDs[5] of conventional GaP- or InAlGaP/GaAs-based materials has been focused on pursuing higher luminous performance (lumens/watt), higher quantum efficiency, and shorter operating wavelength. InAlGaP LEDs[6] grown on GaAs substrates, and then wafer-bonded to transparent GaP, have achieved the current record performance in the red and amber (yellow-orange) spectral regime. For example, the external quantum efficiencies (EQE, η_{ex}) were reported to be higher than 50% and luminous performance to be higher than 50lm/W at λ~610nm. The EQE, however, decreases rapidly, as the wavelength decreases (i.e., with more aluminum content in the active layer), especially further into the green spectral regime. The external quantum efficiencies drop to ~9% in the yellow-orange spectral regime (~595nm) and even to ~2% in yellow-green spectral regime (~570nm)[6], due to the loss of one of the carrier (electrons) from the direct Γ band to the indirect X band, governed by the nature of the InAlGaP band structure. Furthermore, InAlGaP materials are not capable of producing blue light emission due to their relatively small bandgap energy. In contrast to InAlGaP LEDs which have developed from smaller bandgap (red) to wider bandgap (yellow-orange) and which have better performance at smaller bandgap, InGaN LEDs have evolved from the wider bandgap (blue) to smaller bandgap (green). As noted above, IQE is highest in the wavelength of 400~470nm but it decreases rapidly to less than 5% in the wavelength less than 550nm. As a result of the wavelength vs. performance characteristics of InAlGaP and InGaN LEDs, the wavelength regime between 550~580nm remains as a region of "inefficient" LED performance, which is referred to as "the green gap" (Figure 2). Therefore, green LEDs based on InGaN materials have standard of ~525nm peak operating wavelength rather than "true green" 550nm. Decreased efficiency and performance are attributed to excessive strain (hence, quantum confined Stark effect by piezoelectric effect) applied to active layer for green-emitting LEDs. We intend to develop materials growth processes that will provide high-performance InAlGaN LEDs throughout the "green gap". High-efficiency LEDs are projected to provide a dramatic reduction in the power necessary for industrial and commercial lighting and the full implementation of cost-effective high-performance solid-state lighting is projected by 2025 to reduce the electrical power used world-wide for lighting by over 50%[7]. Furthermore, the development of LED-based lighting products would, in the USA alone, (1) save 1.66 Quads of electrical energy; (2) reduce the emission of carbon-containing atmospheric waste by 278M metric tons; and (3) generate a cumulative financial savings of $115B over the period 2000-2020[7].

In this program, we will address the problem of high-efficiency green light emitters using the direct-bandgap InAlGaN quaternary alloy system. Novel epitaxial device structures will be grown using advanced metalorganic chemical vapor deposition (MOCVD) and will be characterized by various structural, optical, electrical characterization techniques, including photoluminescence (PL), electroluminescence (EL), cathodoluminescence (CL), time-resolved PL (TRPL), X-ray diffraction (XRD), transmission electron microscopy (TEM), secondary ion mass spectrometry (SIMS), Rutherford back scattering (RBS), and atomic-force microscopy

(AFM). Light-emitting devices will be designed, fabricated, and tested to optimize their electrical and optical characteristics.

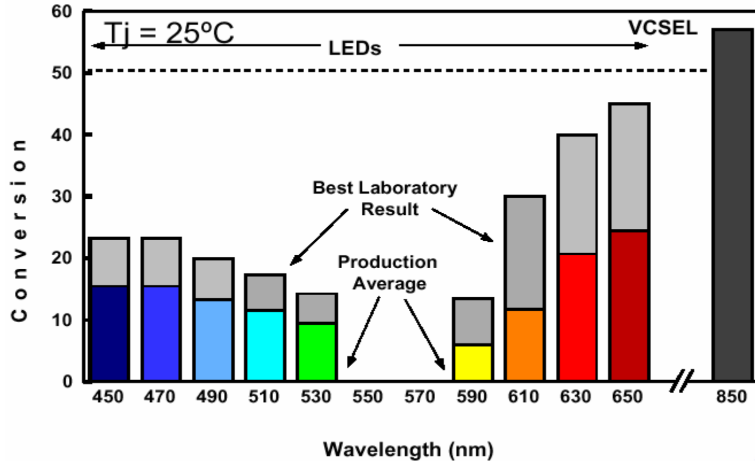

Figure 2: Conversion efficiency vs. wavelength for current generation light-emitting diodes.[8]

In this 36-month project, we are exploring both *INNOVATIVE DEVICE DESIGNS AND MATERAILS GROWTH CONCEPTS*, which will improve the light-emitting capabilities of green LEDs while simultaneously achieving useful optical near-field patterns. These innovative approaches are described in "EXPERIMENTAL" section. The early portion of this program will focus on improved materials growth technologies exploring the use of alternate precursors; the later phases of this program will focus on advanced alternate substrates, e.g., "bulk" GaN and AlN. This work is being performed in collaboration with LumiLeds, a leading USA-based LED manufacturer as an industrial collaborator; a federal research lab, Sandia National Laboratory; as well as a small start-up company that is developing innovative nitride substrates, Crystal IS.

EXECUTIVE SUMMARY

The proposed research program will develop technologies for the growth and fabrication of high-quality green light-emitting devices in the wide-bandgap III-V nitride InAlGaN materials system. This research includes four Tasks: (1) the use of advanced equipment for the MOCVD growth of III-nitride films and the characterization of these materials; (2) the development of innovative growth technologies for high-quality green light-emitting diodes; (3) the study of strain effects and piezoelectric and polarization effects upon the LED performance; (4) the design, fabrication, testing of nitride LEDs. The activities performed during the period from October 2004 to September 2005 for the second year of the program, we have primarily focused on the development/study of (a) high-quality GaN:Mg and InGaN:Mg *p*-type layers that have less/no detrimental thermal annealing effect on green LED active region as well as excellent structural and electrical properties (Task 1 and 2); (b) high-quality InGaN/GaN multiple quantum well (MQW) active region for 520 and 540 nm green LED active region (Task 1, 2, and 3); (c) novel characterization of green LED MQW active region by transmission electron microscopy, electron holography, and cathodoluminescence (Task 3 and 4); (d) the effect of thermal annealing on blue and green LED active region during *p*-type layer growth (Task 4); (e) the comparison of electrical and optical properties of green LEDs employing different *p*-type layers (Task 2 and 4); (f) the design, growth, characterization, and fabrication of green LEDs emitting at 520nm and 540nm (Task 2, 3, and 4), the results of which will be summarized in the "Results and Discussion".

The heterostructures for green LEDs used in this work were grown by low-pressure MOCVD in a commercially manufactured, specially constructed Thomas Swan Close-Coupled Showerhead (CCS) nitride reactor on two-inch diameter *c*-plane (0001) sapphire substrates. The structural, optical, electrical properties of epitaxial heterostructures grown were investigated by a variety of material characterizations: X-ray diffraction (XRD), transmission electron microscopy (TEM), electron holography (EH) secondary ion mass spectrometry (SIMS), transmittance, photoluminescence (PL), wafer-level quick test electroluminescence (EL), cathodoluminescence (CL), time-resolved PL (TRPL), Nomarski optical microscope, atomic-force microscopy (AFM). The fabrication process follows three steps: patterning SiO_2 etch mask, mesa isolation etch (by ICP), and metallization processes (Ti/Al/Ti/Au for *n*-GaN and Ni/Au for *p*-InGaN or *p*-GaN).

The growth optimization for the *p*-type doping of *p*-GaN and *p*-InGaN materials for green LED structure has been carried out as a continued effort from the first year. We achieved a high 300K hole concentration of $p=1.6\times10^{18}$ cm^{-3} and a low resistivity of 0.33 Ω-cm from the sample taht was grown under optimized growth conditions at 1040°C. The $In_{0.04}Ga_{0.96}N$ exhibits a hole concentration of $p=2.0\times10^{18}$ cm^{-3} and a low resistivity of 0.5 Ω-cm.

The essential requirement to achieve high-efficiency green LEDs emitting at long wavelengths is the innovative improvement in high-quality InGaN/GaN multi-quantum well (MQW) active regions. After intensive optimization of the active region growth conditions, PL intensities were dramatically improved in the wavelength range 510~520nm. It is also known that PL and EL have a loose co-relation in terms of luminescence quality especially in green LEDs. After achieving decent quality of active region by PL characterization, EL characterization by quick test was employed for the evaluation of luminescence quality of the LEDs depending on the growth conditions and the structure for the active region.

For the *p*-type layers employed in green LEDs, the thermal annealing effect on the active region during the growth needs to be considered as well as the structural and electrical properties of the layer itself. The electrical and optical characteristics of LEDs employing different *p*-type layers were investigated from PL and electroluminescence (EL). The PL wavelength was blue-shifted and the intensity decreased with increasing growth temperature of the *p*-layer, indicating that optical degradation of the MQW active region occurred due to thermal annealing during growth of the *p*-layer in hydrogen ambient. Only slight decrease in PL intensity was observed, because the low growth temperature and nitrogen ambient of the *p*-layer growth are friendly growth conditions for the InGaN MQW active region. The *I-V* characteristics of the LEDs with a *p*-$In_{0.04}Ga_{0.96}N$ layer and with a *p*-GaN layer. It was found that the turn-on voltages of LEDs with a *p*-$In_{0.04}Ga_{0.96}N$ layer and with a *p*-GaN layer were 2.8 and 2.5 V and 20 mA forward voltages were 3.3 and 3.1 V, respectively, indicating that the LED devices shows very low resistivity with the device size of 230×230 μm^2. However, the higher hole concentration and lower resistivity in the LED with a *p*-$In_{0.04}Ga_{0.96}N$ layer can provide a better current spreading and the series resistance is lower than that of with a *p*-GaN layer, once the diode is turned on.

We have studied on (i) the effect of Si in the QWB of the active region; (ii) the effect of *p*-type layer (GaN:Mg and InGaN:Mg) grown on green LED active region; and (iii) the effect of growth parameter and structural parameter of InGaN/GaN MQW green LED active region by photoluminescence and electroluminescence. Based on the study of various structural and MOCVD growth parameter effects, we have grown several green LED structures (i) with *p*-$In_{0.04}Ga_{0.96}N$ layer and (ii) without Si doping in the QWB (iii) by employing optimized growth parameters for efficient green emitters operating at ~520 and ~540 nm. The purpose of the LED structure growth is for the evaluation/quantification of the improvement and progress that we have made under the NETL green LED program. For the second year review of the program, the issue of difficulties in measuring "true and reliable" internal quantum efficiencies from outside industrial collaborators was raised. As an alternative/complementary solution, the optical power of packaged and unpackaged LED structures together with internal quantum efficiency evaluation will be measured.

EXPERIMENTAL

MOCVD growth of InAlGaN heterostructures for green LEDs

The InAlGaN heterostructures used in this work were grown by low-pressure MOCVD in a commercially manufactured, specially constructed Thomas Swan Close-Coupled Showerhead (CCS) nitride reactor on two-inch diameter *c*-plane (0001) sapphire, 6H-SiC, or smaller (0001) GaN and AlN substrates. The reactor system is designed to have a capability to accommodate up to seven 2.0 in. diameter wafers in one run. Generally, most of the non-In-containing nitride materials were grown in a H_2 ambient employing the primary precursors trimethylgallium (TMGa), triethylgallium (TEGa), trimethylindium (TMIn), and trimethylaluminum (TMAl) as alkyl sources, and ammonia (NH_3) as the hydride source. Silane (SiH_4) and bis(cyclopentadienyl)-magnesium (Cp_2Mg) were employed as *n*-type and *p*-type dopant precursors, respectively. Layers containing indium were typically grown in a N_2 ambient. For the growth of these III-N materials, Dupuis' new laboratory at the Georgia Institute of Technology has two new Thomas Swan CCS 7x2 MOCVD systems dedicated to nitride growth. These systems have the latest technology for the growth of III-N films and have eight or more individual metalorganic sources, e.g., TMGa, TMIn, TEGa, etc., as well as provisions for four hydride sources, e.g., SiH_4, NH_3, etc.

The basic nitride growth technique we employ exploits the advantages of a two-step growth procedure to optimize the optical and electrical characteristics of the materials used to form the LEDs. The first set of operating conditions involved the low-temperature (~550°C), growth of a pseudomorphic ~20 nm thick GaN or AlN buffer layer (BL). Then the temperature was ramped to ~1040-1060°C for the growth of the GaN layers. For the growth of InGaN active layers, the growth temperature of ~700-900°C was employed. *In-situ* monitoring of the reflectivity of the wafer versus time and emissivity-corrected pyrometry by LayTec EpiTT system were employed to monitor growth temperature of the wafer, *in-situ* surface quality, and growth rate of the layers being grown.

In addition to "standard MOCVD growth techniques", using the new nitride MOCVD systems described above, we will explore the growth of InAlGaN quaternaries using a modulated precursor epitaxial growth (MPEG) approach, which involves sequentially exposing the growth surface to a modulated partial pressure of Column III precursors and Column V precursors. This will create an alloy determined by the relative exposures of In, Al, and Ga in separate growth cycles. MPEG-MOCVD can have some advantages for the low-temperature growth of InAlGaN alloys where phase separation is possibly a problem. It also may provide a technique wherein increased In alloy compositions can be reproducibly achieved. This process may also be interesting because the optimal growth conditions for InGaN and AlGaN are dramatically different. Using the MPEG-MOCVD approach, we can expect that the Al, Ga, and In atoms will have a higher mobility at low temperatures, creating a more uniform alloy composition, reduced local strain and concomitant defect density, and smoother surface morphology. Since these low-temperature-grown InAlGaN alloys are a critical element in the demonstration of high-performance ultra-thin QW active regions, the growth rate can be kept small so that the overall device growth time is not strongly impacted by this approach.

Material characterization for green LEDs

The properties of InAlGaN epitaxial heterostructures grown were investigated by a variety of material characterizations. The structural property of the epitaxial layers was characterized by X-ray diffraction (XRD) and transmission electron microscopy (TEM). XRD was employed to study crystalline qualities of GaN buffer and the layers subsequently grown from symmetric and asymmetric rocking curve scan. The line width of the peak on rocking curve scans closely related to mosaic spreading induced by various component of dislocations. XRD was also employed to study composition, thickness, and interface quality of multi-quantum well (MQW) active layers from triple-axis ω-2θ scans in conjunction with simulation based on X-ray dynamical diffraction. Microscopic structural defects and features, such as total and each component dislocation density quantification, interface quality of MQWs, and possible defects induced by strain, InGaN layer, Mg dopant, etc.. The chemical properties of the layers were characterized by secondary ion mass spectrometry (SIMS) and Rutherford back scattering (RBS). SIMS was employed for dopant and impurity depth profiling. For accurate composition evaluation, RBS can be employed, since it does not require calibration of matrix materials. The optical properties of the structures were characterized by transmittance, photoluminescence (PL), quick-test electroluminescence (EL), cathodoluminescence (CL), and time-resolved PL (TRPL). Especially, CL will be used to study the effect of phase separation on optical qualities of the MQWs. The electrical properties of the layers and structures were characterized by Hall measurement and contactless sheet resistance mapping system. Macroscopic and microscopic surface morphology of the layer is investigated by Nomarski optical microscope and atomic-force microscopy (AFM). Scanning electron microscope was employed to estimate the thickness and feature sizes of the hetero-epitaxial layers and device structures.

Device fabrication processing and measurement for green LEDs

The fabrication process follows three important steps; namely, patterning etch mask, mesa isolation etch, and metallization processes. First, pattern by SiO_2 etch mask using conventional lithography and liftoff, followed by mesa isolation with a SiO_2 etch mask using ICP (inductively-coupled plasma) dry etching was performed. The SiO_2 mask exhibits good selectivity (~10:1) over the layer to be etched, when etching GaN. Once the mesa was defined, metallization step followed, by depositing bottom layer (*n*-GaN) ohmic contact which is Ti/Al/Ti/Au. As the last step, *p*-GaN layer ohmic contacts which can be Pd/Au or Ni/Au were deposited. All metallization processes were done by E-beam evaporation. Contact annealing was performed at 500°C for 1minute.

Once fabrication was done, we first characterized the electrical performance using semiconductor parameter analyzer. The quality of ohmic contacts was studied by TLM (transmission line measurement) characterization. Diode *I-V* characteristics were also measured. Electroluminescence (EL) performance characteristics were measured either by a “quick” LED test set up on a epitaxial wafer by using indium dot contacts or by “full” LED testing on processed LEDs.

RESULTS AND DISCUSSION

Development of *p*-type GaN and $In_xGa_{1-x}N$ for green LED *p*-cladding/contact layers

In wide bandgap semiconductor materials and devices as in GaN based systems, *p*-type doping has been one of the major technical challenges and it still requires intensive optimization process to achieve improved performance devices. Mg is the only currently available *p*-type dopant in GaN based MOCVD materials, but it has several technical issues: the activation energy of Mg was reported to be very high (>170 meV); Mg is prone to form electrically inactive Mg-H complexes; Mg can contribute to form anti-domain boundaries, which could disturb local spontaneous polarization field, etc. Also, *p*-type doping of GaN is known to strongly depend on material quality of the layer and background doping level of carbon and oxygen (both can compensate *p*-type doping as deep donors) as well as Mg incorporation level. For controlled *p*-type doping, growth condition of epitaxial layer needs to be calibrated as well as Mg incorporation to achieve optimum growth condition.

The growth optimization for the *p*-type doping of *p*-GaN:Mg and *p*-InGaN:Mg materials for green LED structure has been carried out as a continued effort from the first year. We calibrated and compared electrical properties of the *p*-type layer grown under different growth conditions, especially the growth temperature and indium composition of the layer. Three samples were prepared employing optimized growth condition for a given growth temperature and compositions: sample (a) *p*-$In_{0.04}Ga_{0.96}$:Mg at 840°C, sample (b) *p*-GaN:Mg at 930°C, and sample (c) *p*-GaN:Mg at 1040°C. Figure 3 shows the measured hole concentration, mobility, and resistivity of the samples (a), (b), and (c). A high free-hole concentration of $p=1.6\times10^{18}$ cm^{-3} and a mobility of μ_h~12 $cm^2/V\cdot s$, resulting in a very low resistivity of 0.33 Ω-cm at 300 K for the GaN:Mg sample (c), which was grown under optimized growth condition at 1040°C, were achieved. Secondary ion mass spectroscopy (SIMS) depth profiling for the sample reveals that carbon and oxygen impurity levels are well controlled - very low near detection limit. Variable-temperature Hall data of the GaN:Mg layer shows ~170 meV of activation energy, which is close to the value reported for GaN:Mg activation for *p*-type doping[9]. As the GaN:Mg growth temperature decreased to 940°C, the hole concentration was reduced and the resistivity increased even with optimized growth conditions. Lower resistivity of sample (c) is believed to be due to better crystalline quality and minimized background impurity incorporation, and thus a higher hole mobility, as the growth temperature increases. Figure 5 (b) and (c) shows the AFM images of GaN:Mg samples grown at 940 and 1040°C. The RMS roughness of the samples (b) and (c) were 0.590 nm and 0.318 nm, respectively, for 5×5 μm^2 scans, suggesting material crystalline quality differences between the layers grown at different temperatures. The rougher surfaces obtained at lower growth temperatures can be attributed to the fact that Ga ad-atoms do not have enough energy to migrate to proper lattice sites, thus, lateral growth rate becomes smaller due to the shorter Ga diffusion length[10]. To verify the effect of Ga ad-atom diffusion length on material quality, hence on electrical property of *p*-GaN:Mg layer grown at lower temperatures, *p*-GaN at 930°C was calibrated with reduced growth rate. Figure 4 shows the measured hole concentration, mobility, and resistivity of the *p*-GaN sample grown at 930°C with different growth rate. Higher growth rate sample (Rg~3nm/s) corresponds to sample (b) of Figure 3. As growth rate decreases, hole concentrate and mobility increased and hence conductivity of the sample was improved and we consider that this is due to improved material quality of *p*-GaN layer by decreasing growth rate of the layer grown at lower temperatures. Atomic force

microscope was performed to study the relation between structural quality and electrical property of *p*-layers. For *p*-type InGaN, it is well known that hole concentration can be enhanced as a consequence of reduced activation energy of Mg acceptor in $In_xGa_{1-x}N$ with increasing indium composition, x_{In} [11,12,13]. In this study, sample (a), which is $In_{0.04}Ga_{0.96}N$:Mg grown at 840°C, shows low resistivity with higher hole concentration (p=2.0×10^{18} cm^{-3} and a low resistivity of 0.5 Ω-cm) due to the reduced Mg activation energy, as shown in Figure 3. The sample (a), however, shows lower carrier mobility (μ_h~6 cm^2/V·s) due to less-perfect crystalline quality relative to sample (b) or (c). Such a result suggests that InGaN is a very attractive material for the low resistive *p*-type layer of LED device. The co-relation between electrical properties and materials quality characterized by AFM indicates that the electrical properties of the *p*-layer is closely related to material crystalline quality differences between the layers grown at different temperatures and growth rates. Also, results suggest that further study is needed for InGaN growth condition optimization for *p*-type doping to take a full advantage of reduced activation energy of Mg in InGaN materials.

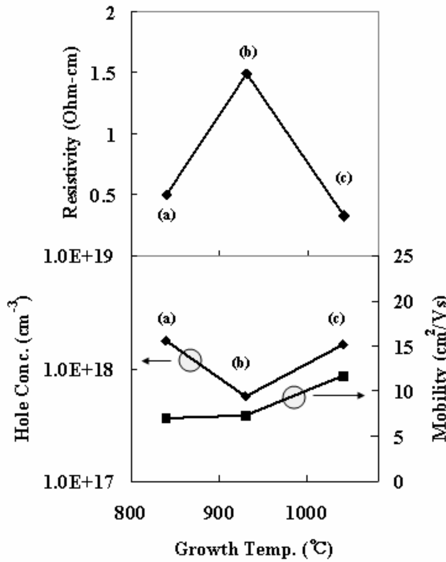

Figure 3: Measured hole concentration, mobility, and resistivity of *p*-$In_{0.04}Ga_{0.99}N$:Mg and *p*-GaN:Mg samples.

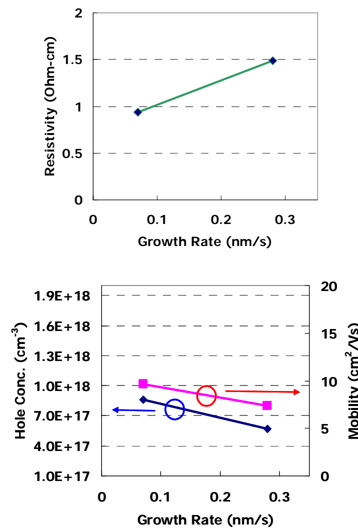

Figure 4: Measured hole concentration, mobility, and resistivity of *p*-GaN:Mg at 930°C with different growth rate.

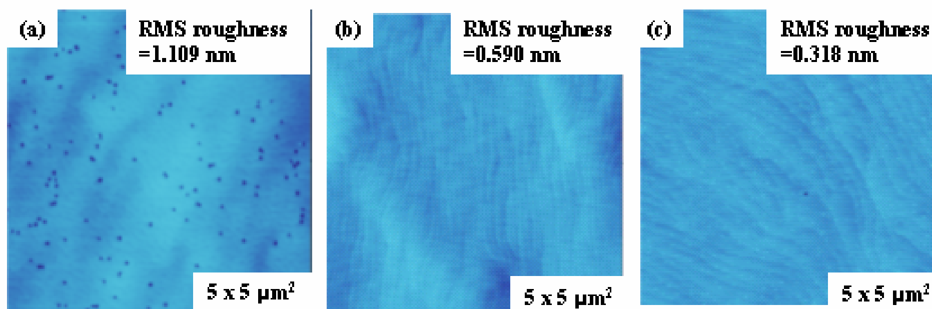

Figure 5: The AFM images with the 5×5 μm^2 scans of *p*-$In_{0.04}Ga_{0.99}N$:Mg and *p*-GaN:Mg samples.

InGaN/GaN MQW active region calibration for green LEDs

The essential requirement to achieve high-efficiency green LEDs emitting at long wavelengths is the innovative improvement in high-quality InGaN/GaN multi-quantum well (MQW) active regions. It is related to the alloy composition, phase separation, doping, and crystalline and interface quality control in InGaN QW and GaN QW barriers, optimization of piezoelectric charge effect in the active region epitaxial structures, etc. The optical quality of green LED active region and the dependence of the luminescence on the growth parameters were characterized by 300K photoluminescence (PL).

For reference, the first study of active-region optimization results (reported on the first year annual report) is shown in Figure 6 (a). We continued green LED active region optimization (the second batch) based on the experience that we have earned from the first optimization studies. The major growth parameters that need to be altered for this second optimization were the growth temperatures of QW and QWB, sacrificing layer insertion between QW and QWB during transition, growth pressure, TMIn flow rate, growth rate (related to TMGa or TEGa flow rate), NH_3 flow rate, etc. The general trend of PL peak wavelength and intensity affected by above growth parameters is that as the PL peak wavelength increases toward the longer-wavelength green visible spectral region by tuning a certain growth parameter, the PL intensity decreases. For example, a decrease in the growth temperature and the growth pressure and an increase in growth rate make the PL peak wavelength longer ("green-shifted") while making PL peak intensity lower. The aim of this second optimization was that of increasing the PL peak wavelength with a minimum decrease in the PL peak intensity by tuning the complicated "inter-linked" growth parameters. Also, we have performed active region calibration from structural point of view, such as QW and QWB thicknesses and Si doping in QWB. Figure 6 (b) shows the PL intensity change with a peak wavelength increase from InGaN/GaN MQWs for the second batch of green LED MQW active region optimization. Note the PL intensities were dramatically improved at comparable wavelengths for this set of optimization parameters, especially in the wavelength range 500~520nm. Also, the PL linewidths of the peaks were decreased, as compared to the first series of MQW active region calibrations.

300K PL was employed for the calibration of active region for green LED structure. We also perform the active region consisting of InGaN/GaN MQW by electroluminescence (EL). It is known that PL and EL have a loose co-relation in terms of luminescence quality especially in green LEDs. After achieving decent quality of active region by PL characterization, EL characterization by quick test was employed for the evaluation of luminescence quality of the LEDs depending on the growth conditions and the structure for the active region. Figure 7 and Figure 8 show the electroluminescence (EL) spectra depending on current injection of two LED structures measured by the LED quick test, exhibiting the EL peak wavelength at 520 nm and 540 nm. Figure 9 summarized the structural, electrical, and optical characterization results of the green LED structures. Note that the contact itself may not be perfect ohmic behavior in the quick test set up, since indium dot contacts were used for both *n*-type and *p*-type contacts. Consequently, voltage levels themselves of this measurement cannot be compared to "fully-processed" devices. Forward voltages of two structures seem to be comparable considering the relatively large error bar of electrical characterization of quick test - electrical characterization will be compared more detail from processed devices. From the EL peak compared at I~50 mA, the peak intensity and peak linewidth are higher (arbitrary unit intensity ~124 vs. 49 for

intensity) and narrower (FWHM in nm ~ 37 vs. 45) for ~520nm LED structures. We also note that wavelength "blue" shift as a function of injection current is much smaller than other typical green LEDs. The detailed analysis for this beneficial reduced blue shift is underway.

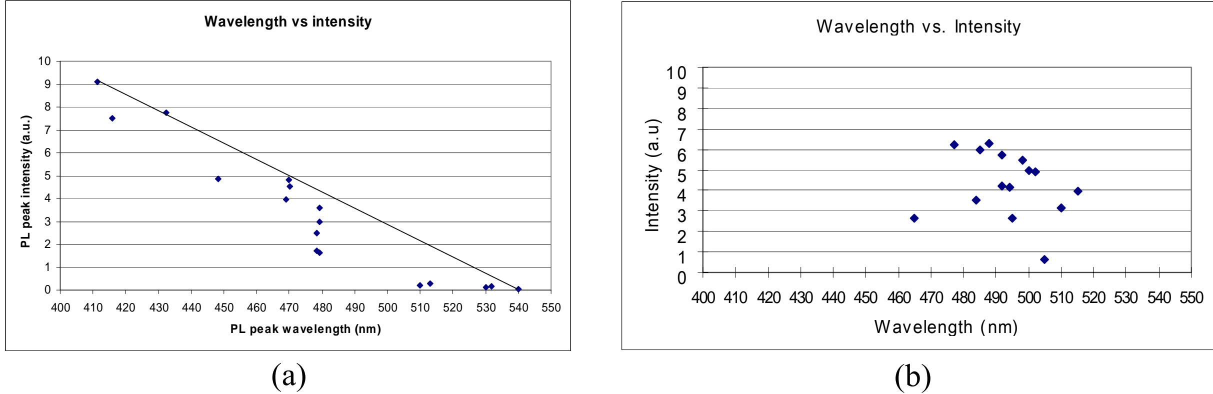

Figure 6: PL intensity change with peak wavelength increase from InGaN/GaN MQWs for (a) the first batch and (b) the second batch of green LED MQW active region optimization.

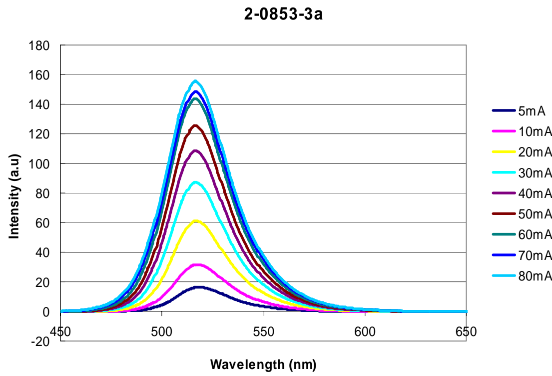

Figure 7: EL intensity change with increasing injection current from InGaN/GaN MQWs of 520nm green LED MQW by quick EL test.

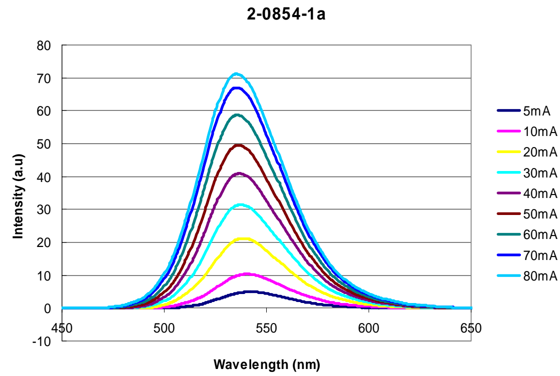

Figure 8: EL intensity change with increasing injection current from InGaN/GaN MQWs of 540nm green LED MQW by quick EL test.

Sample ID	Voltage		EL @50 mA				XRD
	V @20 mA	V @50 mA	Intensity (a.u)	Wavelength (nm)	FWHM (nm)	Wavelength Shift (@ 5- 50mA)	-1st SL peak FWHM (s)
2-0853	7	8.2	124	518	37	2	~215
2-0854	6	7.5	49	538	45	6	~240

Figure 9: Summary of the structural, electrical, and optical characterization results for the green LED structures.

Novel structural characterization of InGaN/GaN MQW active region for green LEDs

We have grown, fabricated, and characterized the green LED structures having different *p*-type layers. The LEDs with different *p*-type layers showed different optical and electrical characteristics while having the same structures in the active region as determined from X-ray diffraction. The microstructures of the LEDs with *p*-GaN and *p*-$In_{0.04}Ga_{0.96}N$ layers were characterized by transmission electron microscopy (TEM) and electron holography. The characterization was carried out in collaboration with Prof. Ponce group at Arizona State University. Figure 10 (a) and (b) are TEM micrographs showing cross-section of multiple

quantum well (MQW active layers for LEDs with *p*-GaN and *p*-$In_{0.04}Ga_{0.96}N$ layers. The quantum well (QW) and quantum well barrier (QWB) have same thickness for both LED structures, which is consistent with X-ray diffraction characterization. The thicknesses were estimated to be ~2.1-2.6nm (8-10 (002) lattice spacing) and ~4.2-4.7nm (16-18 (002) lattice spacing) for QW and QWB, respectively. Also, the interface between QW and QWB has a sharp contrast from the image. The electron holography (EH) characterization technique was employed to obtain the profile of the electrostatic potential within the active region. The holographic phase difference in the TEM is directly proportional to variations of the projected electrostatic potential. Figure 11 shows the EH of MQW active layers for LEDs with *p*-$In_{0.04}Ga_{0.96}N$ layers. EH shows QW fields ~-1MV/cm along the [0001] consistent with 7-11% In composition for InGaN pseudomorphic on GaN. However, the GaN Barriers also show a weak field .1-.2MV/cm suggesting that they are under tensile strain. We believe this could be related to the existence of *p*-$In_{0.04}Ga_{0.96}N$ layers on top of active region. Further investigation of EH characterization is underway and we will report complete characterization of active region for the green LED structure with different *p*-type layers.

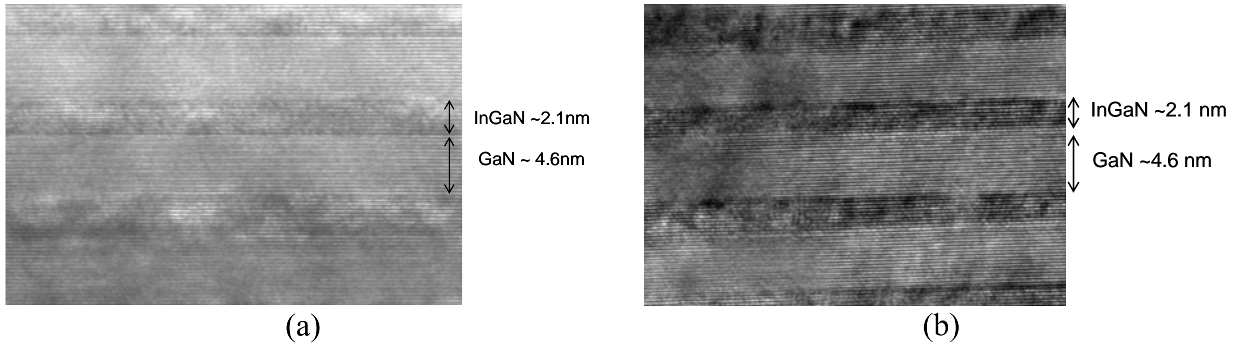

Figure 10: Cross-sectional transmission electron microscopy of MQW active layers for LEDs with (a) *p*-GaN and (b) *p*-$In_{0.04}Ga_{0.96}N$ layers.

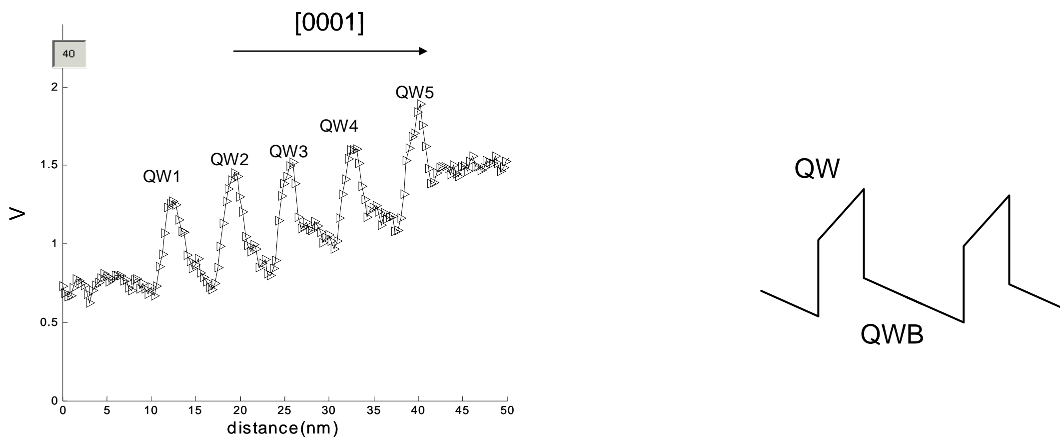

Figure 11: Electron holography of MQW active layers for LEDs with *p*-$In_{0.04}Ga_{0.96}N$ layers.

Effect of thermal annealing during *p*-type layer growth on green LED performance

For the *p*-type layers employed in green LEDs, the thermal annealing effect on the active region during the growth needs to be considered as well as the structural and electrical properties

of the layer itself. The electrical and optical characteristics of LEDs employing different *p*-type layers were investigated from PL and electroluminescence (EL). Four green LED samples were prepared employing different *p*-type layers: sample (d) without any *p*-type layer; sample (e) *p*-$In_{0.04}Ga_{0.96}$:Mg at 840°C; sample (f) *p*-GaN:Mg at 930°C; and sample (g) *p*-GaN:Mg at 1040°C. The optical properties of MQW and LED structures employing *p*-type layers grown under different growth conditions were studied by PL. As shown in Figure 12, the PL wavelength was blue-shifted and the intensity decreased with increasing growth temperature of the *p*-layer (from (e) to (g) in the order of increasing growth temperature for subsequent *p*-layer growth), indicating that optical degradation of the MQW active region occurred due to thermal annealing during growth of the *p*-layer. Especially, no distinct PL peaks from the active region were obtained due to the significant thermal degradation in sample (g). Also, significant structural degradation was observed in sample (g) from XRD as evident from the increase in the FWHM (full-width-at-half-maximum) of the -1st order peak of the InGaN/GaN MQW with increasing growth temperature of *p*-type layers. In the sample with *p*-InGaN grown at 840°C (sample (e)), no decrease in PL intensity was observed. The PL wavelength and intensity of the MQW structure was studied for samples grown at 740°C (sample (d)) and 770°C (sample (h)) for green and blue emitters, respectively. It was found that the wavelength can be shifted from 470 nm to 510 nm, which is attributed to the difference of the indium composition in the well layer. As shown in Figure 13, a decrease of the PL intensity was observed in the green spectral region. The PL intensity of the MQW emission in the green spectral region decreased to ~ 40% in comparison with the intensity in the blue spectral region.

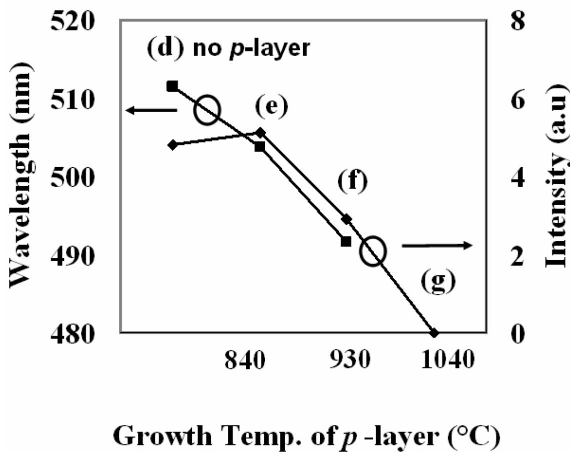

Figure 12: Room-temperature PL wavelength and intensity of MQW and LED samples (d), (e), (f), and (g).

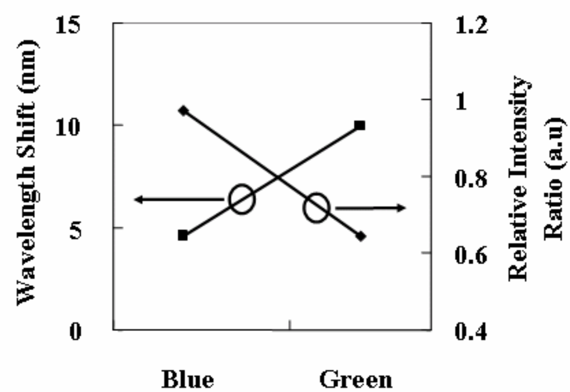

Figure 13: Room-temperature PL wavelength shift and relative intensity ratio of blue and green LEDs.

Electroluminescence comparison of green LEDs having different *p*-type layers

For EL of LEDs with *p*-layers grown at 840°C, 930°C, and 1040°C, the overall peak intensity change depending on *p*-type layer growth condition was consistent with the PL results, indicating the thermal degradation of the MQW active region with the increasing growth temperature of the *p*-layer. Figure 14 shows the room-temperature EL spectra of sample (e) and (f) at low current levels. Note that an EL peak longer than 590 nm (depending on current level) in sample (e), which has *p*-$In_{0.04}Ga_{0.96}N$ layer, was observed, while such peaks could not be

observed in sample (f) which has a *p*-GaN layer. This EL peak at the long-wavelength side was dominant at 3 and 5 mA and became saturating at ~15 mA. At a higher current level than 15 mA, another EL peak appeared at 530 nm and increased and then became dominant as the current level increased. Again such a peak at longer wavelength was not observed for LEDs with a *p*-GaN layer. We believe this additional peak at the longer-wavelength side (λ>590 nm) for the sample (e) is originated from piezoelectric effect induced in the *p*-InGaN layer, while the peak developed later at high current levels is related to MQW active region. This peak cannot be observed in PL spectrum due to the mechanism of the hole transport. Figure 15 shows EL spectra from sample (e) and (f) at higher current levels. As expected, the *p*-$In_{0.04}Ga_{0.96}N$ layer-related EL peak becomes negligible and only the MQW related EL peak can be observed. The EL intensity of sample (e) with a *p*-$In_{0.04}Ga_{0.96}N$ layer is much better than that of sample (f) with a *p*-GaN layer. In sample (e), this enhanced hole injection into the active region and the current spreading may be responsible for the improvement of the EL intensity. Also, a more serious thermal degradation of the MQW in sample (f) is another reason for the lower EL intensity. Figure 16 shows the *I-V* characteristics of the LED Sample (e) with a *p*-$In_{0.04}Ga_{0.96}N$ layer and sample (f) with a *p*-GaN layer. It was found that the turn-on voltages of sample (e) and (f) were 2.5 and 2.8 V and 20 mA forward voltages were 3.1 and 3.3 V, respectively, indicating that the LED devices shows very low resistivity with the device size of 230×230 μm^2. It can be explained that the higher voltage in sample (e) could originate from the hole barrier in the *p*-InGaN and GaN QW barrier interface. However, the higher hole concentration and lower resistivity in the sample (e) can provide a better current spreading and the series resistance is lower than that of sample (f), once the diode is turned on. We propose to design a LED structure with indium composition grading *p*-$In_{0.04}Ga_{0.96}N$ layer to GaN barrier in order to solve this problem.

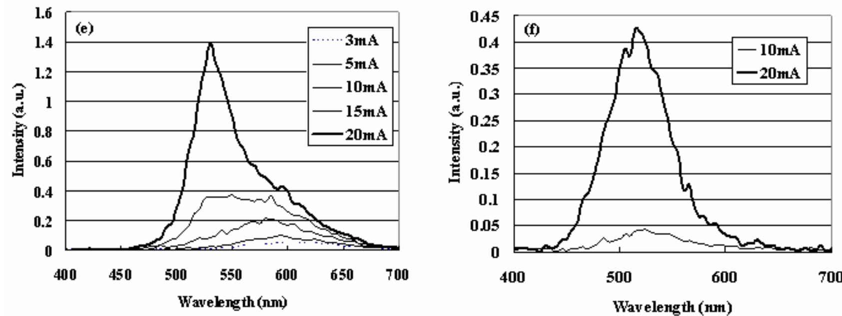

Figure 14: The room-temperature EL spectra of LED Sample (e) and (f) at low current level.

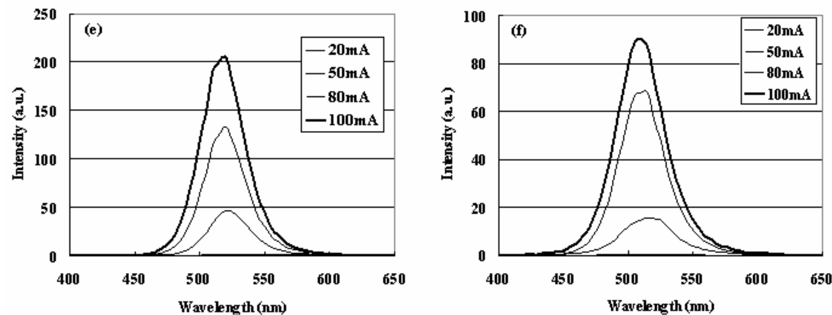

Figure 15: The room-temperature EL spectra of LED Sample (e) and (f) at high current level.

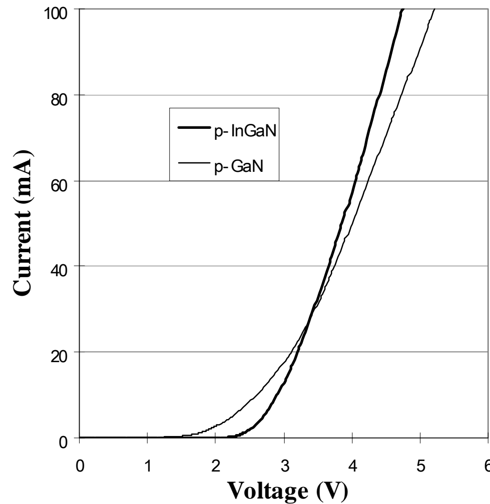

Figure 16: Current-voltage characteristics of green LEDs with different *p*-layers at room temperature.

InGaN:Mg contact (20 nm)
InGaN:Mg (50 nm)
GaN QWB (8.5 nm)
InGaN QW (4 nm)
GaN QWB (8.5 nm)
GaN:Si+ (40 nm)
GaN:Si- (300 nm)
GaN:Si+ (1000 nm)
GaN:Si (2700 nm)
GaN:nid (1100 nm)
sapphire

(a)

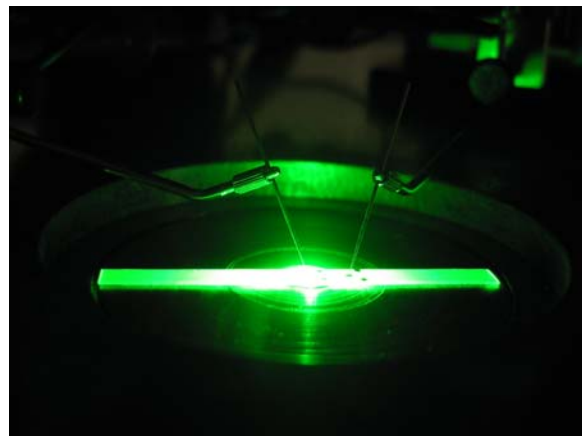

(b)

Figure 17: (a) Schematic epitaxial structure of the green LEDs grown for the optical power measurement and internal quantum efficiency evaluation and (b) Bright luminescence emitting at 540nm from green LED epitaxial structure by EL quick test.

Growth and fabrication of LEDs with different wavelengths

We have studied on (1) the effect of Si in the QWB of the active region; (2) the effect of *p*-type layer (GaN:Mg and InGaN:Mg) grown on green LED active region; and (3) the effect of growth parameter and structural parameter of InGaN/GaN MQW green LED active region by photoluminescence and electroluminescence. Based on the study of various structural and MOCVD growth parameter effects, we have grown several green LED structures (i) with *p*-$In_{0.04}Ga_{0.96}N$ layer and (ii) without Si doping in the QWB (iii) by employing optimized growth parameters for efficient green emitters operating at ~520 and ~540 nm. The purpose of the LED structure growth is for the evaluation/quantification of the improvement and progress that we have made under the NETL green LED program. For the second year review of the program, the issue of difficulties in measuring “true and reliable” internal quantum efficiencies from outside

industrial collaborators was raised. As an alternative/complementary solution, the optical power of packaged and unpackaged LED structures together with internal quantum efficiency evaluation will be measured. Figure 17 shows schematic epitaxial structure of the green LEDs. The LED structures grown have been sent to multiple industrial collaborators for the performance evaluation in terms of optical power and internal quantum efficiency.

CONCLUSION

The proposed research program will develop technologies for the growth and fabrication of high-quality green light-emitting devices in the wide-bandgap III-V nitride InAlGaN materials system. This research includes four Tasks: (1) the use of advanced equipment for the MOCVD growth of III-nitride films and the characterization of these materials; (2) the development of innovative growth technologies for high-quality green light-emitting diodes; (3) the study of strain effects and piezoelectric and polarization effects upon the LED performance; (4) the design, fabrication, testing of nitride LEDs. The activities performed during the period from October 2004 to September 2005 for the second year of the program, we have primarily focused on the development/study of (a) high-quality GaN:Mg and InGaN:Mg *p*-type layers that have less/no detrimental thermal annealing effect on green LED active region as well as excellent structural and electrical properties; (b) high-quality InGaN/GaN multiple quantum well (MQW) active region for 520 and 540 nm green LED active region; (c) novel characterization of green LED MQW active region by transmission electron microscopy, electron holography, and cathodoluminescence; (d) the effect of thermal annealing on blue and green LED active region during *p*-type layer growth; (e) the comparison of electrical and optical properties of green LEDs employing different *p*-type layers; (f) the design, growth, characterization, and fabrication of green LEDs emitting at 520nm and 540nm.

We have grown green LEDs with peak EL wavelengths at 520nm and 540nm. The LED consists of InGaN/GaN MQW and *p*-InGaN layers. The measurement of the relative internal quantum efficiencies and optical power of LED wafers/devices we have prepared is being carried out for the quantitative evaluation of progress of green LEDs during the second year of the program.

LIST OF ACRONYMS AND ABBREBIATIONS

AFM	Atomic force microscopy
arc-s	arc-second
CCS	Close-coupled showerhead
CL	Cathodoluminescence
(Cp_2Mg)	Bis(cyclopentadienyl)-magnesium
C-V	Capacitance-Voltage
E-beam	Electron beam
EBL	Electron blocking layer
EH	Electron Holography
EL	Electroluminescence
EQE	External quantum efficiency
ICP	Inductively-coupled plasma
IQE	Internal quantum efficiency
I-V	Current-Voltage
FWHM	Full-width at half maximum
LED	Light emitting diode
L-I	Light-Current
MiRC	Microelectronics Research Center
MPEG	Modulated precursor epitaxial growth
MOCVD	Metalorganic chemical vapor deposition
MQW	Multi-quantum well
PL	Photoluminescence
QW	Quantum well
QWB	Quantum well barrier
RBS	Rutherford back scattering
RTA	Rapid thermal annealing
SEM	Scanning electron microscopy (or microscope)
SIMS	Secondary ion mass spectroscopy
TEGa	Triethylgallium
TMAl	Trimethylaluminum
TMGa	Trimethylgallium
TMIn	Trimethylindium
TEM	Transmission electron microscopy (or microscope)
TLM	Transmission line measurement
TRPL	Time-resolved photoluminescence
UV	Ultraviolet
XRD	X-ray diffraction (or diffractometer)

BIBLIOGRAPHY

Journal Publication

1. J. B. Limb, W. Lee, J. H. Ryou, D. Yoo, and R. D. Dupuis, "Comparison of GaN and $In_{0.04}Ga_{0.96}N$ *p*-layers on the electrical and electroluminescence properties of green light emitting diodes," *J. Appl. Phys.* (submitted for publication).
2. J. B. Limb, W. Lee, J.-H. Ryou, D. Yoo, T. Chung, and R. D. Dupuis, "Electrical and optical properties of green LEDs employing low temperature grown $In_xGa_{1-x}N$:Mg," *Phys. Stat. Sol. (a)* (submitted for publication).
3. Wonseok Lee, Jae Limb, Jae-Hyun Ryou, Dongwon Yoo, Theodore Chung, and Russell D. Dupuis, "Influence of growth temperature and growth rate of *p*-GaN layers on the characteristics of green light emitting diodes," *J. Electron. Mater*. (in press in April issue of 2006).
4. Wonseok Lee, Jae Limb, Jae-Hyun Ryou, Dongwon Yoo, Theodore Chung, and Russell D. Dupuis, "Effect of thermal annealing induced by *p*-type layer growth on blue and green LED performance," *J. Crystal Growth* **287**, 577 (2006).

Conference Presentation

5. Wonseok Lee, Jae Limb, Jae-Hyun Ryou, Dongwon Yoo, Michael Stevens, Sridhar Srinivasan, Fernando Ponce, and Russell D. Dupuis, "Characterization of green LED structures with *p*-InGaN and *p*-GaN layers," *EMC 2006 (48th Electronic Materials Conference)*, University Park, Pennsylvania, Jun, 2006. (accepted).
6. Wonseok Lee, Jae Limb, Jae-Hyun Ryou, Dongwon Yoo, and Russell D. Dupuis, "Optoelectronic characteristics and electronic structure comparison of green LEDs with *p*-InGaN and *p*-GaN " (B3.05)," *ISBLLED 2006 (6th International Symposium of Blue Laser and Light Emitting Diodes)*, Montpellier, France, May, 2006.
7. (Invited talk) W. Lee, J. Limb, J. H. Ryou, D. Yoo, T. Chung, and Russell D. Dupuis, "Growth of green lighting emitting diodes by MOCVD" (B1), *Optics in the Southeast-2005*, Atlanta, Georgia, Oct. 2005.
8. W. Lee, J.-H. Ryou, and R.D. Dupuis, "Post-growth thermal annealing effects on the properties of InGaN/InGaN and InGaN/GaN multi-quantum-wells" (Th-P-061), *The 6th International Conference on Nitride Semiconductors (ICNS-6)*, Bremen, Germany, Aug.~Sep. 2005.
9. Wonseok Lee, Jae Limb, Jae-Hyun Ryou, Dongwon Yoo, Ted Chung, and Russell Dupuis "Effect of thermal annealing induced by p-type layer growth on blue and green LED performance," *12th US Biennial Workshop on Organometallic Vapor Phase Epitaxy (OMVPE 2005)*, Big Sky, Montana, Jul. 2005.
10. Wonseok Lee, Jae Limb, Jae-Hyun Ryou, Dongwon Yoo, Ted Chung, and Russell Dupuis "Effect of gallium precursor on InGaN/GaN multi-quantum wells and Mg-doped layer for green LEDs" (A5), *47th Electronic Materials Conference (EMC2005)*, Santa Barbara, California, Jun. 2005.

REFERENCES

[1] M. Krames, DoE Workshop on Solid State Lighting, 2003.

[2] T. Matsuoka, H. Okamoto, M. Nakao, H. Harima, and E. Kurimoto, "Optical bandgap energy of wurtzite InN," App. Phys. Lett. **81**, 1246 (2002).

[3] Group III Nitride Semiconductor Compounds, edited by B. Gil, Oxford University Press, Oxford UK (1998).

[4] S. Muthu, F. J. P. Schurman, and M. D. Pashley, "Red, green, and blue LEDs for white light illumination," IEEE J. Select. Topic Quantum Electron. **8**, 333 (2002).

[5] M. G. Craford, "LEDs challenge the incandescents, IEEE Circuit and Device Mag. **8**, 24 (1992).

[6] D. A. Vanderwater, I. H. Tan, G. E. Hofler, D. C. Defevere, and F. A. Kish, "High-brightness InAlGaP light emitting diodes," Proc. IEEE **85**, 1752 (1997).

[7] "*The Promise of Solid State Lighting for General Illumination—2002 Update*," DoE BTS and OIDA (Published by OIDA, Washington DC, 2002).

[8] This diagram is obtained from the LumiLeds website, http://www.lumileds.com/pdfs/techpaperspres/SPIE2001.PDF.

[9] W. Gotz, N. M. Johnson, J. Wlker, D. P. Bour, and R. A. Street, Appl. Phys. Lett. **68**, 667 (1996).

[10] S. Kitamura, K. Hiramatsu, and N. Sawaki, Jpn. J. Appl. Phys. **34**, L184 (1995).

[11] K. Kumakura, T. Makimoto, and N. Kobayashi, J. Crystal Growth **221**, 267 (2000).

[12] K. Kumakura, T. Makimoto, and N. Kobayashi, J. Appl. Phys. **93**, 3370 (2003)..

[13] S.-N. Lee, T. Sakong, W. Lee, H. Paek, J. Son, E. Yoon, K. Nam, and Y. Park, . Crystal Growth **261**, 249 (2004).